THE JOURNAL OF PHYSICAL CHEMISTRY LETTERS
A JOURNAL OF THE AMERICAN CHEMICAL SOCIETY

pubs.acs.org/JPCL Letter

Photoluminescence Blinking and Biexciton Auger Recombination in Single Colloidal Quantum Dots with Sharp and Smooth Core/Shell Interfaces

Wenli Guo,[‖] Jialun Tang,[‖] Guofeng Zhang,* Bin Li, Changgang Yang, Ruiyun Chen, Chengbing Qin, Jianyong Hu, Haizheng Zhong, Liantuan Xiao,* and Suotang Jia

Cite This: *J. Phys. Chem. Lett.* 2021, 12, 405−412 Read Online

ABSTRACT: There is an inconsistence on whether a smooth core/shell interface can reduce Auger recombination and suppress photoluminescence (PL) blinking in single colloidal quantum dots (QDs). Here, we investigate the influence of a core/shell interface on PL blinking and biexciton Auger recombination by comparing the single-dot PL spectra of $Cd_xZn_{1-x}Se_yS_{1-y}$/ZnS core/shell QDs with sharp and smooth interfaces. The inconsistence can be clarified when considering different PL blinking mechanisms. For the single QDs showing Auger blinking, a smooth core/shell interface potential can suppress PL blinking through reducing the Auger recombination. In contrast, we find slightly reduced biexciton Auger recombination rates but increased PL blinking activities in the band-edge carrier (BC)-blinking QDs with the smooth core/shell interface. This is because the smooth interface potential cannot reduce the PL blinking caused by the transfer of electrons to the surface states; however, there is potential to increase electron wave function delocalization for reducing the biexciton Auger recombination rate.

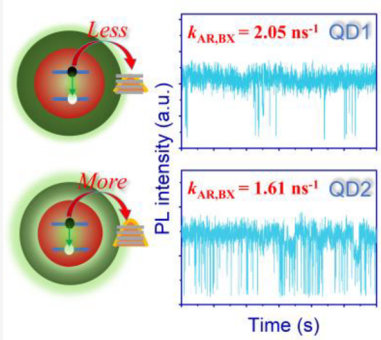

Colloidal semiconductor quantum dots (QDs) show superior optical properties including high photoluminescence (PL) quantum yields (QYs), broad absorption, and narrow emission spectra,[1−5] making them promising materials for light-emitting diodes,[6,7] lasers,[8] photovoltaic devices,[9−11] single-photon sources,[12] and biomedical labels.[13−15] Nonetheless, almost all single colloidal QDs exhibit PL blinking,[16−20] the random switching between bright (on) and dim/dark (off) states, which is a considerable drawback in QD-based applications, e.g., degrading the performance of lasers and light-emitting diodes,[21] interrupting the photon emission of quantum light sources,[22] and causing difficulty in single-particle tracking.[23]

In the pioneering work of Efros, PL blinking has been explained by a charging model due to photoionization and neutralization of QDs.[24] Under a constant photoexcitation, the QD undergoes photoionization to form a charged QD. The charged QD couples with the next-generated electron−hole pair to create a negative or positive trion state to initiate efficient Auger recombination as nonradiative decay processes.[24,25] Auger recombination quenches the PL emission via passing the exciton energy to a third carrier (either electron or hole). As a result, the PL emission of the trion states is significantly lower than that of the bright state. Therefore, the bright state of the PL intensity trajectory can be attributed to the radiative recombination in a neutral QD, and the off state is due to the nonradiative Auger recombination in a charged QD. This type of blinking behavior is denoted as Auger blinking.[16] The PL blinking of single QDs reported initially was mainly associated with the nonradiative Auger recombination.[26] The sharp core/shell interface of a QD makes the Auger processes more frequently take place.[27] Therefore, the gradient or uniform alloy layers were employed to smoothen the core/shell interface of QDs for suppressing the Auger recombination.[27−29] These alloy layers result in a soft confinement potential, which affects both electrons and holes, thus increasing the biexciton PLQY by suppressing the nonradiative biexciton Auger recombination.[30] Giant CdSe−$CdSe_{1-x}S_x$ core-alloyed-shell QDs have been demonstrated to be a better system for suppressing nonradiative Auger-recombination-induced PL blinking.[31] However, it has also been reported that the suppression of Auger recombination and PL blinking in small QDs are entirely independent of soft confinement potentials.[32−36]

Besides Auger blinking, the other blinking-mechanism—surface-trap-induced nonradiative recombination also results in PL blinking of QDs.[16] In this mechanism, the shallow surface traps, also known as multiple recombination centers

Received: October 7, 2020
Accepted: December 17, 2020

Table 1. Detailed Parameters of the Fabricated $Cd_xZn_{1-x}Se_yS_{1-y}$/ZnS Core/Shell QDs

	shell growth temperature (°C)	core diameter (nm)	QD size (nm)	no. ZnS shell monolayers	peak of PL spectra (nm)	fwhm of PL spectra (nm)	PLQY (%)
QD1	220	7.4	10.7	3	544.6	27.8	69
QD2	280	7.4	10.6	3	514.0	29.8	84
QD3	280	7.4	9.1	2	515.2	29.2	82
QD4	280	7.4	8.0	1	517.2	30.0	65

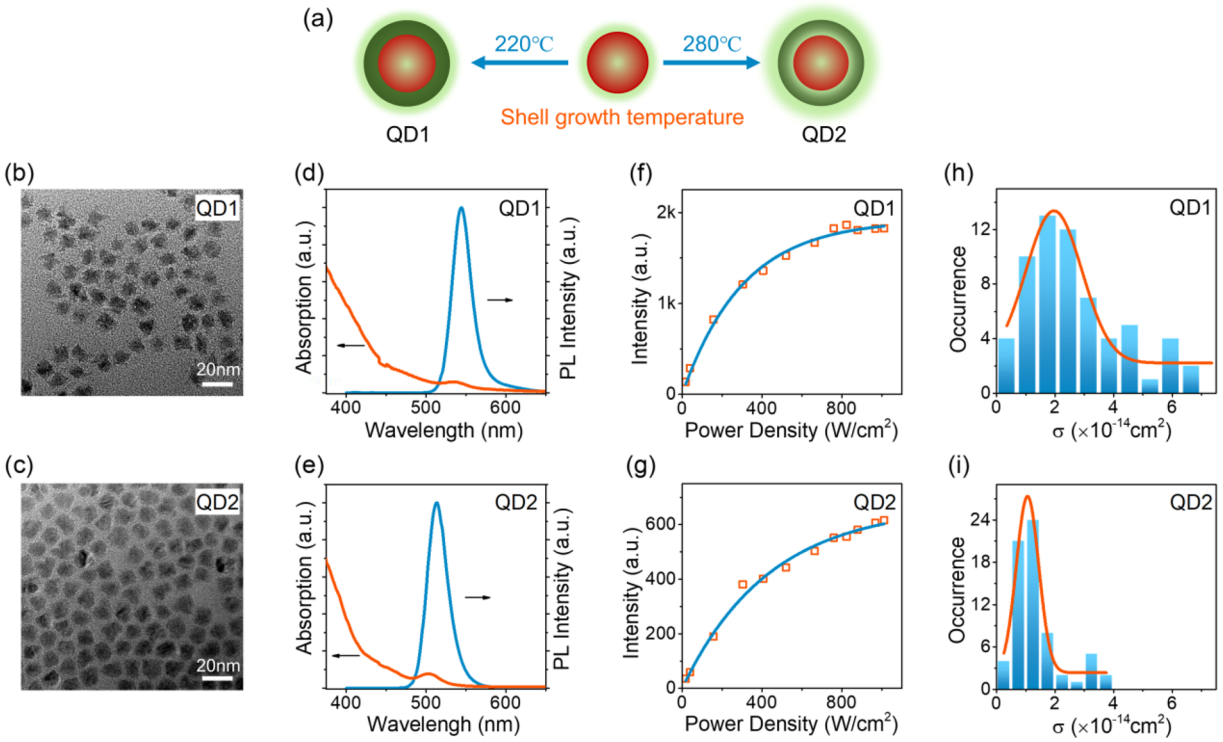

Figure 1. (a) Schematic illustration of QD synthesis at different shell-growth temperatures. The dark and bright core/shell interfaces represent the sharp and smooth interface potentials for QD1 and QD2, respectively. (b, c) Transmission electron microscopy (TEM) micrographs for QD1 and QD2. (d, e) Optical absorption and PL emission spectra of QD1 and QD2 in toluene. (f, g) The PL saturation curves for single QD1 and single QD2. (h, i) Histograms of absorption cross sections for single QD1s and single QD2s and the corresponding Gaussian fitting curves.

(MRCs),[37] provide nonradiative channels for band-edge carriers. The random activation and deactivation of the MRCs cause a constantly changing nonradiative recombination rate and hence PL blinking. This type of blinking is termed as band-edge carrier (BC) blinking. Like Auger blinking, BC blinking generally occurs in the CdSe-based core/shell QDs, but the off states of the BC blinking are generated by nonradiative recombination through the MRCs in a neutral QD, without undergoing the Auger processes.

We speculate that the reduction of Auger recombination may not be associated with the suppression of PL blinking in the BC-blinking QDs. In order to clarify the discrepancy in the literature reports and to verify our hypothesis, here, we use a series of gradient alloyed $Cd_xZn_{1-x}Se_yS_{1-y}$/ZnS QDs, with pure BC blinking, to investigate the effects of the sharp and smooth core/shell interfaces on PL blinking and biexciton Auger recombination in single QDs. By applying different temperatures for shell growth, we synthesized $Cd_xZn_{1-x}Se_yS_{1-y}$/ZnS QDs with the sharp and smooth core/shell interfaces. These QDs allow us to explore the influence of different interfacial potentials on PL blinking. The absorption cross sections of single QDs are measured from their PL saturation curves. Normalized by the QDs' absorption cross sections, the average number of photons absorbed per QD per pulse ($\langle N \rangle$) for the single QDs with different interfacial potentials is set to the same level in our time-tagged, time-resolved, and time-correlated single-photon counting (TTTR-TCSPC) measurements. Comparing the differences in the time-resolved PL information, we find that the previously reported discrepant observations in the literature can be clarified when considering different PL blinking mechanisms. For Auger-blinking QDs, a smooth interface potential can suppress PL blinking through reducing the Auger recombination. On the other hand, the smooth core/shell in the BC-blinking QDs increases PL blinking of single QDs, although biexciton Auger recombination can be slightly reduced.

The gradient alloyed $Cd_xZn_{1-x}Se_yS_{1-y}$/ZnS core/shell QDs with 1, 2, and 3 monolayers of ZnS shells were synthesized at shell-growth temperatures of 280 and 220 °C, as summarized in Table 1. The detailed synthesis protocol is described in the Supporting Information (SI). This synthetic approach minimizes the lattice mismatch at the core/shell interface and thus minimizes the interface trap-related PL blinking.[38,39] Table 1 summarizes the key parameters of the resulting $Cd_xZn_{1-x}Se_yS_{1-y}$/ZnS core/shell QDs including synthesis temperatures, core diameters, sizes of QDs, number of ZnS shell monolayers, PL peaks, full-width at half-maximum (fwhm) of the emission spectra, and PLQYs. The QDs with

https://dx.doi.org/10.1021/acs.jpclett.0c03065
J. Phys. Chem. Lett. 2021, 12, 405−412

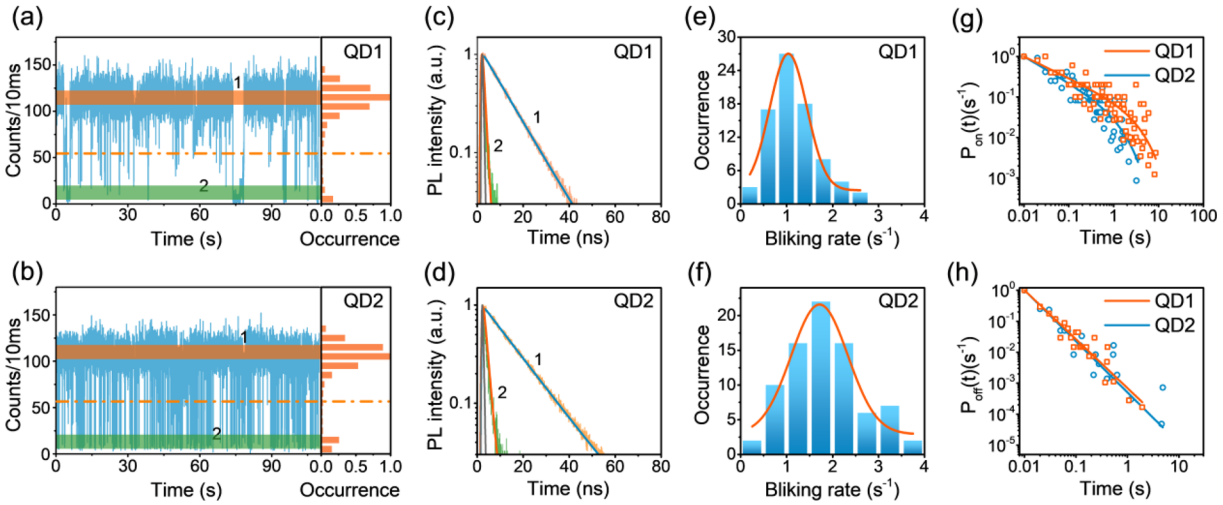

Figure 2. (a, b) Typical PL trajectories for a single QD1 and a single QD2. The right panels show the corresponding PL intensity histograms. (c, d) Corresponding PL decay curves obtained from the PL regions marked in respective colors on PL intensity trajectories of (a,b), respectively. The solid gray lines are the instrument response function of the system. (e, f) Histograms of PL blinking rates for single QD1 and single QD2 obtained under the excitation of the same $\langle N \rangle$. (g) Normalized on-state probability densities for a single QD1 and a single QD2. Fitting parameters for QD1: $\alpha_{on} = 0.53$, $1/\mu_{on} = 3.88$; fitting parameters for single QD2: $\alpha_{on} = 0.64$, $1/\mu_{on} = 1.56$. (h) Normalized off-state probability densities for single QD1 and single QD2. Fitting parameters for single QD1: $\alpha_{off} = 1.58$; fitting parameters for single QD2: $\alpha_{off} = 1.65$.

three monolayer ZnS shells synthesized at the shell-growth temperatures of 220 and 280 °C are marked as QD1 and QD2, respectively (Figure 1a). Figures 1b and 1c show the transmission electron microscope (TEM) images of these two samples. The average sizes of QD1 and QD2 are 10.7 and 10.6 nm, respectively. QD1, synthesized at a relatively low shell-growth temperature, possesses a sharp core/shell interface, while QD2 has a smooth core/shell interface due to the interdiffusion of ions at the higher shell-growth temperature.[40] The gradient and smooth interface of the QD2 have been verified by the elemental distribution analysis of the energy dispersive spectra, as presented in previous literature.[5] Figures 1d and 1e show the absorption and emission spectra of QD1 and QD2 in toluene, respectively. The emission peaks of QD1 and QD2 are 544.6 and 514.0 nm, respectively. The blue-shifted spectrum of the QD2 further confirms that the smooth alloyed core/shell interface was created as a result of the diffusion of Zn atoms into the core.[40,41]

To compare the PL blinking and biexciton Auger recombination between single QD1 and single QD2, we measured the single-dot PL spectra of QD1 and QD2 under the excitation of the same $\langle N \rangle$. Here $\langle N \rangle = \sigma j$ represents the average number of photons absorbed by each QD per pulse, where σ is the absorption cross-section of individual QD and j is the excitation photon flux.[42,43] In order to perform the excitation at the same $\langle N \rangle$, we first determined the absorption cross sections of single QD1 and single QD2 by fitting their PL saturation curves.[44,45] Single QD was excited using a 406 nm picosecond pulsed laser, and PL photons were recorded by the TTTR-TCSPC card. More details about the experimental setup and procedures are given in the Supporting Information. Typical PL saturation curves of single QD1 and single QD2 are shown in Figures 1f and 1g. During the measurement, *p*-phenylenediamine was used to reduce PL intermittency of single QDs and protect them from photobleaching at higher laser power densities.[20] By fitting these PL saturation curves, we extract the σ values of single QDs (see SI for details). The histograms of σ values are presented in Figures 1h and 1i, showing the mean values of 1.96×10^{-14} cm^2 and 1.06×10^{-14} cm^2 for QD1 and QD2, respectively. Therefore, the σ of a single QD1 is approximately twice that of a single QD2. The σ values of QD1 and QD2 were used to normalize $\langle N \rangle$ by setting the 406 nm laser with different j in the PL measurements.

Figures 2a and 2b present the typical PL intensity trajectories (left panels) measured under the excitation of $\langle N \rangle = \sim 0.1$ for a single QD1 and a single QD2, respectively, with the corresponding PL intensity histograms in the right panels. The corresponding fluorescence lifetime-intensity distribution (FLID) maps for the single QD1 and the single QD2 are shown in Figures S1c and S1d. The FLID maps with the small occurrence probability of the gray and dim states are not with sufficient photon statistics to distinguish the blinking mechanism. Therefore, we use radiative lifetime scaling to determine the blinking mechanism of QDs.[16] Figures 2c and 2d present two typical PL decay curves obtained from bright- and dim-state PL regions marked by respective colors in the PL intensity trajectories of Figures 2a and 2b. The solid gray lines in the figures represent the instrument response function (IRF) of a system with a fwhm of about 750 ps. By using the decay-fit program (PicoQuant GmbH), the IRF can be reconvoluted and the corresponding PL lifetimes can be obtained by fitting decay curves with single-exponential functions. Using the lifetime value and the PL intensity, the radiative lifetime scaling is calculated to be ~1.0 for both single QD1 and single QD2 (see SI for details), indicating the PL blinking of QD1 and QD2 to be BC blinking.[16] In a BC-blinking process, the hot exciton first relaxes to the band edge, and then, the electron or hole is captured by a short-lived shallow surface trap. Hence, the time scale of trapping and nonradiative recombination is considered to be close to that of radiative recombination of the band-edge exciton, leading to a characteristic scaling value of 1.[16,46]

According to the two peaks of PL intensity histograms in the right panels of Figures 2a and 2b, a threshold intensity (dotted lines in the figures) was set to separate the on and off state of PL trajectories. The histograms of the blinking rates (the number of blinking events per second)[17] for more than 100 single QD1s and single QD2s are shown in Figures 2e and 2f.

https://dx.doi.org/10.1021/acs.jpclett.0c03065
J. Phys. Chem. Lett. 2021, 12, 405−412

The Gaussian fitting yields the mean values of 1.04 and 1.73 Hz, respectively. It is clear that the PL blinking of single QD2s is more frequent than that of single QD1s.

As another way to compare the blinking behaviors, we calculated on- and off-state probability densities $P_i(t)$ according to the equation:[47] $P_i(t) = \frac{N_i(t)}{N_{i,\text{total}}} \times \frac{1}{\Delta t_{i,\text{av}}}$ (i = on or off). $N_i(t)$ represents the statistics of on- or off-state events in the duration time of t, $N_{i,\text{total}}$ is the total number of on- or off-state events, and $\Delta t_{i,\text{av}}$ is the average of the time intervals to the preceding and following events. The normalized on- and off-state probability densities $P_{\text{on}}(t)$ and $P_{\text{off}}(t)$ of single QD1 and single QD2 are shown in Figures 2g and 2h. The on-state probability densities $P_{\text{on}}(t)$ are well fitted by a truncated power law $P_{\text{on}}(t) = A_{\text{on}}t^{-\alpha_{\text{on}}} \exp(\mu_{\text{on}}t)$, and the off-state probability densities $P_{\text{off}}(t)$ are fitted by a power law $P_{\text{off}}(t) = A_{\text{off}}t^{-\alpha_{\text{off}}}$,[21,48] where $A_{\text{on/off}}$ is the amplitude, $\alpha_{\text{on/off}}$ is the power-law exponent, and μ_{on} is the saturation rate. The fitting methods for the on- and off-state probability densities are the same as those reported in previous literature.[20,21,48,49] The average fitting parameters α and μ were obtained by fitting of more than 100 single QD1s and single QD2s respectively, as shown in Table 2. The single QD1s have a larger $1/\mu_{\text{on}}$ value (5.25 ± 4.59) than that of single QD2s (2.40 ± 1.85), which suggests increased probability densities of long on-state events for single QD1s. Therefore, the observations align with our hypothesis that the QDs with a smooth interface have more blinking, while the QDs with the sharp interface can effectively suppress the blinking.

Table 2. Fitting Parameters of Probability Densities of the On and Off States

	α_{on}	$1/\mu_{\text{on}}$	α_{off}
QD1	0.52 ± 0.32	5.25 ± 4.59	1.51 ± 0.31
QD2	0.55 ± 0.21	2.40 ± 1.85	1.67 ± 0.21
QD3	0.59 ± 0.29	2.31 ± 3.21	1.55 ± 0.27
QD4	1.03 ± 0.29	2.69 ± 3.52	1.47 ± 0.17

We also investigated the PL blinking behaviors of single QDs with 2 and 1 monolayers of ZnS shells at the shell-growth temperature of 280 °C. The 2-layer and 1-layer ZnS shell QDs are marked as QD3 and QD4, respectively. Typical PL trajectories are shown in Figure S2a. The PL blinking behaviors of single QDs with different shell thicknesses are compared by calculating the on- and off-state probability densities. The on- and off-state probability densities of single QD2, single QD3, and single QD4 are shown in Figures S2b and S2c. Table 2 summarizes the average fitting parameters. The parameters of α_{on} decreased from 1.03 ± 0.29 to 0.55 ± 0.21 for the QDs with increasing shell thickness (from QD4 to QD2), indicating that the probability densities of on-state events increased with the increasing ZnS shell thickness. This reveals that the blinking phenomenon is associated with the overlap of wave functions between exciton and surface traps. For QD4 with one monolayer of ZnS shell, the large overlap of exciton wave function and surface trap wave function results in poor photostability.[38] Single QD2 with three monolayers of ZnS shells has a smaller α_{on} and a larger α_{off} than that of the 2-layer QD3, as shown in Table 2. This could be because the thicker shell of QD2 reduces the probability of carriers being captured by the surface traps due to the decreased overlap of wave functions.[38]

We have confirmed in the above that the smooth interface cannot suppress the BC blinking of single QDs. Next, we investigate the effects of the sharp and smooth core/shell interfaces on the biexciton Auger recombination in the BC-blinking QDs. Although the BC blinking does not involve Auger recombination, the biexciton Auger recombination dominates biexciton decay in the BC-blinking QDs. Figure 3a shows a typical PL decay curve of the on-state PL region of

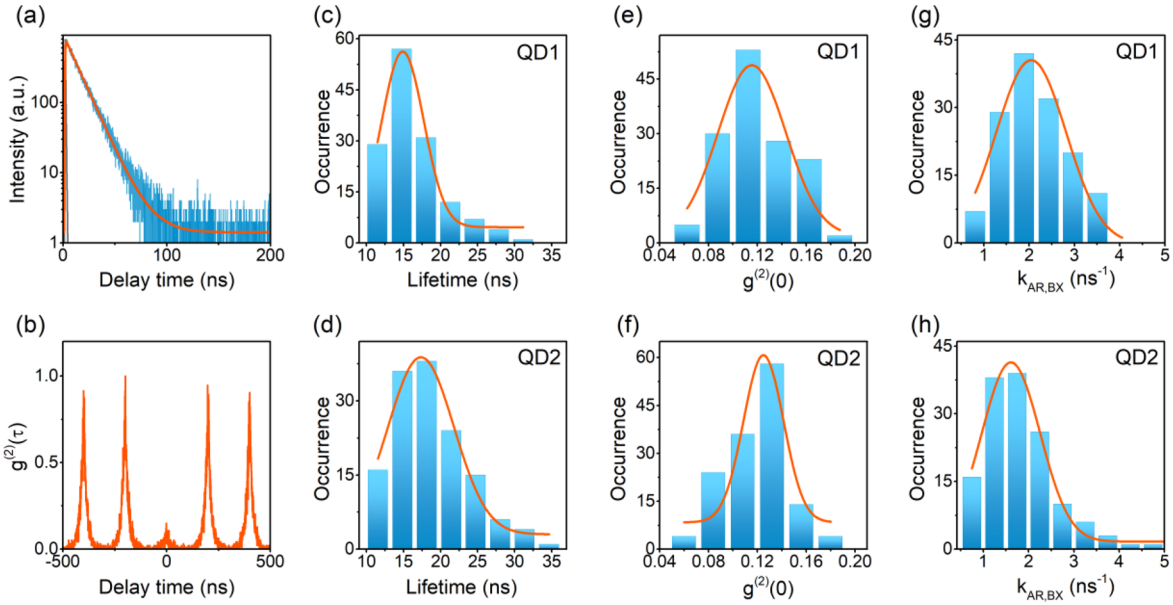

Figure 3. (a) Typical PL decay curve of on-state PL region for single QDs. The solid gray line is the instrument response function of the system. (b) Typical second-order correlation function ($g^{(2)}$) curve of the on-state PL region for single QDs. (c, d) Histograms of single exciton lifetime and corresponding Gaussian fitting curves for single QD1s and single QD2s, respectively. (e, f) Histograms of $g^{(2)}(0)$ values and corresponding Gaussian fitting curves for single QD1s and single QD2s, respectively. (g, h) Histograms of biexciton Auger recombination rates and corresponding Gaussian fitting curves for single QD1s and single QD2s, respectively.

https://dx.doi.org/10.1021/acs.jpclett.0c03065
J. Phys. Chem. Lett. 2021, 12, 405−412

a single QD. By fitting the PL decay curve with a single-exponential function, we can obtain the single-exiton lifetime.[20,49] Figures 3c and 3d show the corresponding histograms of single-exciton lifetimes. The Gaussian fitting yields the mean values of 14.9 and 17.4 ns for single QD1s and single QD2s, respectively. The longer single-exciton lifetime of QD2 than that of QD1 is due to the smooth interface potential of QD2 increasing the delocalization of the electron wave function. Figure 3b shows a typical $g^{(2)}$ curve of the on state of the PL intensity trajectory with a low $g^{(2)}(0)$ value, indicating that the investigated QD is indeed a single nanoparticle.[42,50] The $g^{(2)}(0)$ value can be determined by the ratio of central peak area and side peak area of the $g^{(2)}$ curve. The histograms of $g^{(2)}(0)$ values are shown in Figures 3e and 3f. The mean values, determined by Gaussian fitting, are 0.116 and 0.125 for single QD1s and single QD2s, respectively. Under the weak excitation of $\langle N \rangle = \sim 0.1$, the biexciton QY can be calculated by the equation:[51]

$$\frac{\eta_{BX}}{\eta_X} = g^{(2)}(0) \tag{1}$$

where η_{BX} and η_X are the biexciton QY and single-exciton QY, respectively. The single-exciton QY of the on-state PL intensity trajectory is assumed to be unity for both single QDs.[51] According to eq 1, the biexciton QYs of single QD1 and single QD2 can be calculated as 0.116 and 0.125, respectively. Therefore, the smooth interface potential has little influence on the biexciton QY, which is consistent with the recent report on CdSe/CdS core/shell QDs.[52]

When $\langle N \rangle \ll 1$, the biexciton lifetime of a single QD can be calculated by the equation:[30]

$$g^{(2)}(0) = 4\frac{\tau_{BX}}{\tau_X} \tag{2}$$

where τ_{BX} and τ_X are the biexciton and single-exciton lifetimes, respectively. The biexciton QY can be expressed by the equation:

$$\eta_{BX} = \frac{k_{r,BX}}{k_{r,BX} + k_{AR,BX}} = \frac{k_{r,BX}}{1/\tau_{BX}} \tag{3}$$

where $k_{r,BX}$ and $k_{AR,BX}$ are the biexciton radiative rate and biexciton Auger recombination rate, respectively. The values for η_{BX} and τ_{BX} can be calculated by eqs 1 and 2, respectively; therefore, $k_{AR,BX}$ can be obtained by eq 3. The histograms of $k_{AR,BX}$ are presented in Figures 3g and 3h. Gaussian fitting reveals the mean Auger recombination rates of 2.05 ns^{-1} and 1.61 ns^{-1} for single QD1 and single QD2, respectively. A summary table of the photophysical parameters for single QD1 and single QD2 obtained in this work is presented in Table S1. To sum up, a larger single-exciton lifetime, an almost unchanged biexciton QY, and a slightly reduced biexciton Auger recombination rate are observed for single QD2 with a smooth interface, in comparison with that of single QD1 with a sharp interface.

The schematic illustration of conduction bands (CB) and valence bands (VB) of QD1 and QD2 as well as their surface traps is shown in Figure 4. The schematic diagrams of the CB and VB represent the "abrupt" and "soft" confined profiles for QD1 and QD2, respectively. Although QD1 has the same shell thickness and similar surface traps as that of QD2, the core/shell structure of QD1 has a sharp interface potential between the narrow-bandgap $Cd_xZn_{1-x}Se_yS_{1-y}$ core and the wide-bandgap ZnS shell. The sharp interface would efficiently confine the wave function of the excitons within the core and inner portion of the shells to hold back nonradiative recombination through the MRCs.[53] Therefore, a single QD1 shows reduced PL-blinking events. For the smooth interface potential, the carriers easily eject out to be captured by the surface traps to cause more blinking.[53] On the other hand, the smooth interface potential of QD2 increases electron wave function delocalization to slightly reduce the biexciton Auger recombination rate. The result is consistent with the recent report that the smooth confinement potential can affect the Auger recombination rates by the way of altering wave function delocalization.[52] In addition, QD1 and QD2 show the ensemble PLQYs of 69% and 84%, respectively (Table 1). The lower PLQY of QD1 may be due to more dark particles in the sample.[54] We also tested their stability against photobleaching and found that the survival probability of single QD1 with a sharp interface is higher than that of single QD2 under the excitation of the same $\langle N \rangle$, as presented in Figure S3.

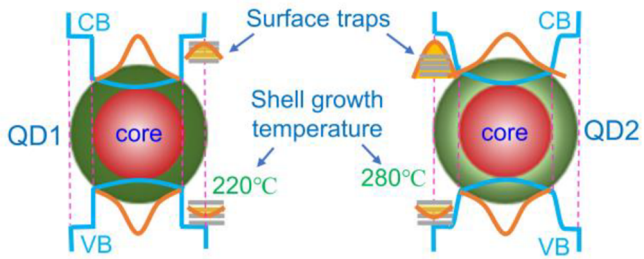

Figure 4. Schematic illustration of conduction bands (CB) and valence bands (VB) of $Cd_xZn_{1-x}Se_yS_{1-y}$/ZnS core/shell QDs with shell growth temperatures at 220 and 280 °C. The bright core/shell interface of QD2 represents a smooth interface potential. The gray lines outside the QDs indicate the surface traps of the QDs, and the yellow shaded wave packets on the gray lines depict the relative probabilities for the carriers to be captured by the surface states.

In summary, we have investigated the effects of the interface potential on PL blinking and the biexciton Auger recombination rate in single $Cd_xZn_{1-x}Se_yS_{1-y}$/ZnS core/shell QDs. The QDs with different interface potentials have the same blinking mechanism (pure BC blinking), confirmed by the radiative lifetime scaling of ~1.0. We find that the single QDs with a smooth interface show more frequent blinking but slightly reduced biexciton Auger recombination rates than that of the single QDs with a sharp interface. This is because the smooth interface potential has a less restrictive effect on electrons, making electrons more easily captured by surface states to cause more blinking. The smooth interface potential results in electron wave function delocalization and the slightly reduced biexciton Auger recombination rate. The various inconsistencies in the previous reports can be clarified by considering different blinking mechanisms. For the Auger-blinking QDs, the smooth interface potential reduces Auger recombination, thereby suppressing the PL blinking. For the BC-blinking QDs, the blinking mechanism does not involve Auger recombination, and therefore, the smooth interface potential reduces the biexciton Auger recombination but does not suppress the blinking. The investigation of the single-dot PL spectroscopy gives a deep insight into the roles of sharp and smooth interface potential, suggesting the rational design of QDs with different interface potential for various applications.

https://dx.doi.org/10.1021/acs.jpclett.0c03065
J. Phys. Chem. Lett. 2021, 12, 405−412

■ ASSOCIATED CONTENT

Supporting Information

The Supporting Information is available free of charge at https://pubs.acs.org/doi/10.1021/acs.jpclett.0c03065.

Sample preparation and characterization, experimental setup, determination of absorption cross-section and estimation of ⟨*N*⟩, BC-blinking determined by radiative lifetime scaling, and the survival probability of single QDs (PDF)

■ AUTHOR INFORMATION

Corresponding Authors

Guofeng Zhang − *State Key Laboratory of Quantum Optics and Quantum Optics Devices, Institute of Laser Spectroscopy, Collaborative Innovation Center of Extreme Optics, Shanxi University, Taiyuan 030006, China;* orcid.org/0000-0002-9030-0431; Email: guofeng.zhang@sxu.edu.cn

Liantuan Xiao − *State Key Laboratory of Quantum Optics and Quantum Optics Devices, Institute of Laser Spectroscopy, Collaborative Innovation Center of Extreme Optics, Shanxi University, Taiyuan 030006, China;* orcid.org/0000-0003-2690-6460; Email: xlt@sxu.edu.cn

Authors

Wenli Guo − *State Key Laboratory of Quantum Optics and Quantum Optics Devices, Institute of Laser Spectroscopy, Collaborative Innovation Center of Extreme Optics, Shanxi University, Taiyuan 030006, China;* orcid.org/0000-0002-3753-7202

Jialun Tang − *Beijing Key Laboratory of Nanophotonics and Ultrafine Optoelectronic Systems, School of Materials Science and Engineering, Beijing Institute of Technology, Beijing 100081, China*

Bin Li − *State Key Laboratory of Quantum Optics and Quantum Optics Devices, Institute of Laser Spectroscopy, Collaborative Innovation Center of Extreme Optics, Shanxi University, Taiyuan 030006, China; Key Laboratory of Spectral Measurement and Analysis of Shanxi Province, College of Physics and Information Engineering, Shanxi Normal University, Linfen 041004, China;* orcid.org/0000-0002-5817-6792

Changgang Yang − *State Key Laboratory of Quantum Optics and Quantum Optics Devices, Institute of Laser Spectroscopy, Collaborative Innovation Center of Extreme Optics, Shanxi University, Taiyuan 030006, China*

Ruiyun Chen − *State Key Laboratory of Quantum Optics and Quantum Optics Devices, Institute of Laser Spectroscopy, Collaborative Innovation Center of Extreme Optics, Shanxi University, Taiyuan 030006, China;* orcid.org/0000-0002-0037-856X

Chengbing Qin − *State Key Laboratory of Quantum Optics and Quantum Optics Devices, Institute of Laser Spectroscopy, Collaborative Innovation Center of Extreme Optics, Shanxi University, Taiyuan 030006, China;* orcid.org/0000-0002-6822-5113

Jianyong Hu − *State Key Laboratory of Quantum Optics and Quantum Optics Devices, Institute of Laser Spectroscopy, Collaborative Innovation Center of Extreme Optics, Shanxi University, Taiyuan 030006, China*

Haizheng Zhong − *Beijing Key Laboratory of Nanophotonics and Ultrafine Optoelectronic Systems, School of Materials Science and Engineering, Beijing Institute of Technology, Beijing 100081, China;* orcid.org/0000-0002-2662-7472

Suotang Jia − *State Key Laboratory of Quantum Optics and Quantum Optics Devices, Institute of Laser Spectroscopy, Collaborative Innovation Center of Extreme Optics, Shanxi University, Taiyuan 030006, China*

Complete contact information is available at: https://pubs.acs.org/10.1021/acs.jpclett.0c03065

Author Contributions

[‖]These authors contributed equally.

Notes

The authors declare no competing financial interest.

■ ACKNOWLEDGMENTS

This project is sponsored by the National Key Research and Development Program of China (2017YFA0304203), the Natural Science Foundation of China (62075120, 61527824, 61675119, 61875109, 91950109, 62075122), the NSFC-STINT (62011530133), the PCSIRT (IRT_17R70), the Natural Science Foundation of Shanxi Province (201901D111010(ZD)), and by the Research Project Supported by Shanxi Scholarship Council of China (HGKY2019002), PTIT, 1331KSC, and 111 Project (D18001).

■ REFERENCES

(1) Zhang, G. F.; Peng, Y. G.; Xie, H. Q.; Li, B.; Li, Z. J.; Yang, C. G.; Guo, W. L.; Qin, C. B.; Chen, R. Y.; Gao, Y.; Zheng, Y. J.; Xiao, L. T.; Jia, S. T. Linear Dipole Behavior of Single Quantum Dots Encased in Metal Oxide Semiconductor Nanoparticles Films. *Front. Phys.* **2019**, *14*, 23605.

(2) Tang, J. L.; Li, F.; Yang, G. L.; Ge, Y.; Li, Z. H.; Xia, Z. G.; Shen, H. B.; Zhong, H. Z. Reducing the Chromaticity Shifts of Light-Emitting Diodes Using Gradient-Alloyed $Cd_xZn_{1-x}Se_yS_{1-y}$@ZnS Core Shell Quantum Dots with Enhanced High-Temperature Photoluminescence. *Adv. Opt. Mater.* **2019**, *7*, 1801687.

(3) Wang, H.; Wang, Z.; Xiong, Y.; Kershaw, S. V.; Li, T.; Wang, Y.; Zhai, Y.; Rogach, A. L. Hydrogen Peroxide Assisted Synthesis of Highly Luminescent Sulfur Quantum Dots. *Angew. Chem., Int. Ed.* **2019**, *58*, 7040−7044.

(4) Ghimire, S.; Sivadas, A.; Yuyama, K.; Takano, Y.; Francis, R.; Biju, V. Quantum Dot-Polymer Conjugates for Stable Luminescent Displays. *Nanoscale* **2018**, *10*, 13368−13374.

(5) Tang, J. L.; Huang, S.; Li, Z. H.; Shen, H. B.; Lv, Z.; Zhong, H. Z. Morphology Evolution of Gradient-Alloyed $Cd_xZn_{1-x}Se_yS_{1-y}$@ZnS Core-Shell Quantum Dots During Transmission Electron Microscopy Determination: A Route to Illustrate Strain Effects. *J. Phys. Chem. C* **2018**, *122*, 4583−4588.

(6) Dai, X. L.; Deng, Y. Z.; Peng, X. G.; Jin, Y. Z. Quantum-Dot Light-Emitting Diodes for Large-Area Displays: Towards the Dawn of Commercialization. *Adv. Mater.* **2017**, *29*, 1607022.

(7) Zhang, W. L.; Prodanov, M. F.; Schneider, J.; Gupta, S. K.; Dudka, T.; Vashchenko, V. V.; Rogach, A. L.; Srivastava, A. K. Ligand Shell Engineering to Achieve Optimal Photoalignment of Semiconductor Quantum Rods for Liquid Crystal Displays. *Adv. Funct. Mater.* **2019**, *29*, 1805094.

(8) Fan, F. J.; Voznyy, O.; Sabatini, R. P.; Bicanic, K. T.; Adachi, M. M.; McBride, J. R.; Reid, K. R.; Park, Y. S.; Li, X. Y.; Jain, A.; Quintero-Bermudez, R.; Saravanapavanantham, M.; Liu, M.; Korkusinski, M.; Hawrylak, P.; Klimov, V. I.; Rosenthal, S. J.; Hoogland, S.; Sargent, E. H. Continuous-Wave Lasing in Colloidal Quantum Dot Solids Enabled by Facet-Selective Epitaxy. *Nature* **2017**, *544*, 75−79.

(9) Etgar, L.; Yanover, D.; Capek, R. K.; Vaxenburg, R.; Xue, Z. S.; Liu, B.; Nazeeruddin, M. K.; Lifshitz, E.; Gratzel, M. Core/Shell

PbSe/PbS QDs TiO_2 Heterojunction Solar Cell. *Adv. Funct. Mater.* **2013**, *23*, 2736−2741.
(10) Li, B.; Chen, R.; Qin, C.; Yang, C.; Guo, W.; Han, X.; Gao, Y.; Zhang, G.; Xiao, L.; Jia, S. Interfacial Charge Transfer between $CsPbBr_3$ Quantum Dots and ITO Nanoparticles Revealed by Single-Dot Photoluminescence Spectroscopy. *Appl. Phys. Express* **2019**, *12*, 112003.
(11) Talgorn, E.; Gao, Y. N.; Aerts, M.; Kunneman, L. T.; Schins, J. M.; Savenije, T. J.; van Huis, M. A.; van der Zant, H. S. J.; Houtepen, A. J.; Siebbeles, L. D. A. Unity Quantum Yield of Photogenerated Charges and Band-Like Transport in Quantum-Dot Solids. *Nat. Nanotechnol.* **2011**, *6*, 733−739.
(12) Aharonovich, I.; Englund, D.; Toth, M. Solid-State Single-Photon Emitters. *Nat. Photonics* **2016**, *10*, 631−641.
(13) Fan, Y. Y.; Liu, H. L.; Han, R. C.; Huang, L.; Shi, H.; Sha, Y. L.; Jiang, Y. Q. Extremely High Brightness from Polymer-Encapsulated Quantum Dots for Two-Photon Cellular and Deep-Tissue Imaging. *Sci. Rep.* **2015**, *5*, 9908.
(14) Mandal, G.; Darragh, M.; Wang, Y. A.; Heyes, C. D. Cadmium-Free Quantum Dots as Time-Gated Bioimaging Probes in Highly-Autofluorescent Human Breast Cancer Cells. *Chem. Commun.* **2013**, *49*, 624−626.
(15) Biju, V.; Itoh, T.; Ishikawa, M. Delivering Quantum Dots to Cells: Bioconjugated Quantum Dots for Targeted and Nonspecific Extracellular and Intracellular Imaging. *Chem. Soc. Rev.* **2010**, *39*, 3031−3056.
(16) Yuan, G. C.; Gomez, D. E.; Kirkwood, N.; Boldt, K.; Mulvaney, P. Two Mechanisms Determine Quantum Dot Blinking. *ACS Nano* **2018**, *12*, 3397−3405.
(17) Li, B.; Zhang, G. F.; Wang, Z.; Li, Z. J.; Chen, R. Y.; Qin, C. B.; Gao, Y.; Xiao, L. T.; Jia, S. T. Suppressing the Fluorescence Blinking of Single Quantum Dots Encased in N-Type Semiconductor Nanoparticles. *Sci. Rep.* **2016**, *6*, 32662.
(18) Han, X.; Zhang, G.; Li, B.; Yang, C.; Guo, W.; Bai, X.; Huang, P.; Chen, R.; Qin, C.; Hu, J.; Ma, Y.; Zhong, H.; Xiao, L.; Jia, S. Blinking Mechanisms and Intrinsic Quantum-Confined Stark Effect in Single Methylammonium Lead Bromide Perovskite Quantum Dots. *Small* **2020**, 2005435.
(19) Li, B.; Zhang, G.; Zhang, Y.; Yang, C.; Guo, W.; Peng, Y.; Chen, R.; Qin, C.; Gao, Y.; Hu, J.; Wu, R.; Ma, J.; Zhong, H.; Zheng, Y.; Xiao, L.; Jia, S. Biexciton Dynamics in Single Colloidal CdSe Quantum Dots. *J. Phys. Chem. Lett.* **2020**, *11*, 10425−10432.
(20) Yang, C. G.; Zhang, G. F.; Feng, L. H.; Li, B.; Li, Z. J.; Chen, R. Y.; Qin, C. B.; Gao, Y.; Xiao, L. T.; Jia, S. T. Suppressing the Photobleaching and Photoluminescence Intermittency of Single near-Infrared CdSeTe/ZnS Quantum Dots with P-Phenylenediamine. *Opt. Express* **2018**, *26*, 11889−11902.
(21) Pietryga, J. M.; Park, Y. S.; Lim, J. H.; Fidler, A. F.; Bae, W. K.; Brovelli, S.; Klimov, V. I. Spectroscopic and Device Aspects of Nanocrystal Quantum Dots. *Chem. Rev.* **2016**, *116*, 10513−10622.
(22) Efros, A. L.; Nesbitt, D. J. Origin and Control of Blinking in Quantum Dots. *Nat. Nanotechnol.* **2016**, *11*, 661−671.
(23) Jaqaman, K.; Loerke, D.; Mettlen, M.; Kuwata, H.; Grinstein, S.; Schmid, S. L.; Danuser, G. Robust Single-Particle Tracking in Live-Cell Time-Lapse Sequences. *Nat. Methods* **2008**, *5*, 695−702.
(24) Efros, A. L.; Rosen, M. Random Telegraph Signal in the Photoluminescence Intensity of a Single Quantum Dot. *Phys. Rev. Lett.* **1997**, *78*, 1110−1113.
(25) Wang, L. W.; Califano, M.; Zunger, A.; Franceschetti, A. Pseudopotential Theory of Auger Processes in CdSe Quantum Dots. *Phys. Rev. Lett.* **2003**, *91*, 056404.
(26) Javaux, C.; Mahler, B.; Dubertret, B.; Shabaev, A.; Rodina, A. V.; Efros, A. L.; Yakovlev, D. R.; Liu, F.; Bayer, M.; Camps, G.; Biadala, L.; Buil, S.; Quelin, X.; Hermier, J. P. Thermal Activation of Non-Radiative Auger Recombination in Charged Colloidal Nanocrystals. *Nat. Nanotechnol.* **2013**, *8*, 206−212.
(27) Bae, W. K.; Padilha, L. A.; Park, Y. S.; McDaniel, H.; Robel, I.; Pietryga, J. M.; Klimov, V. I. Controlled Alloying of the Core-Shell Interface in CdSe/CdS Quantum Dots for Suppression of Auger Recombination. *ACS Nano* **2013**, *7*, 3411−3419.
(28) Park, Y. S.; Bae, W. K.; Pietryga, J. M.; Klimov, V. I. Auger Recombination of Biexcitons and Negative and Positive Trions in Individual Quantum Dots. *ACS Nano* **2014**, *8*, 7288−7296.
(29) Park, Y. S.; Lim, J.; Makarov, N. S.; Klimov, V. I. Effect of Interfacial Alloying Versus "Volume Scaling" on Auger Recombination in Compositionally Graded Semiconductor Quantum Dots. *Nano Lett.* **2017**, *17*, 5607−5613.
(30) Park, Y. S.; Bae, W. K.; Padilha, L. A.; Pietryga, J. M.; Klimov, V. I. Effect of the Core/Shell Interface on Auger Recombination Evaluated by Single-Quantum-Dot Spectroscopy. *Nano Lett.* **2014**, *14*, 396−402.
(31) Nasilowski, M.; Spinicelli, P.; Patriarche, G.; Dubertret, B. Gradient CdSe/CdS Quantum Dots with Room Temperature Biexciton Unity Quantum Yield. *Nano Lett.* **2015**, *15*, 3953−3958.
(32) Cao, H. J.; Ma, J. L.; Huang, L.; Qin, H. Y.; Meng, R. Y.; Li, Y.; Peng, X. G. Design and Synthesis of Antiblinking and Antibleaching Quantum Dots in Multiple Colors Via Wave Function Confinement. *J. Am. Chem. Soc.* **2016**, *138*, 15727−15735.
(33) Qin, W.; Liu, H.; Guyot-Sionnest, P. Small Bright Charged Colloidal Quantum Dots. *ACS Nano* **2014**, *8*, 283−291.
(34) Chen, O.; Zhao, J.; Chauhan, V. P.; Cui, J.; Wong, C.; Harris, D. K.; Wei, H.; Han, H. S.; Fukumura, D.; Jain, R. K.; Bawendi, M. G. Compact High-Quality CdSe-CdS Core-Shell Nanocrystals with Narrow Emission Linewidths and Suppressed Blinking. *Nat. Mater.* **2013**, *12*, 445−451.
(35) Dziatkowski, K.; Ratchford, D.; Hartsfield, T.; Li, X.; Gao, Y.; Tang, Z. CdSe/ZnS Colloidal Quantum Dots with Alloyed Core/Shell Interfaces: A Photoluminescence Dynamics Study. *Acta Phys. Pol., A* **2011**, *120*, 870−873.
(36) Jain, A.; Voznyy, O.; Hoogland, S.; Korkusinski, M.; Hawrylak, P.; Sargent, E. H. Atomistic Design of CdSe/CdS Core-Shell Quantum Dots with Suppressed Auger Recombination. *Nano Lett.* **2016**, *16*, 6491−6496.
(37) Frantsuzov, P. A.; Volkan-Kacso, S.; Janko, B. Model of Fluorescence Intermittency of Single Colloidal Semiconductor Quantum Dots Using Multiple Recombination Centers. *Phys. Rev. Lett.* **2009**, *103*, 207402.
(38) Huang, B.; Yang, H.; Zhang, L.; Yuan, Y.; Cui, Y.; Zhang, J. Effect of Surface/Interfacial Defects on Photo-Stability of Thick-Shell CdZnSeS/ZnS Quantum Dots. *Nanoscale* **2018**, *10*, 18331−18340.
(39) Bae, W. K.; Nam, M. K.; Char, K.; Lee, S. Gram-Scale One-Pot Synthesis of Highly Luminescent Blue Emitting $Cd_{1-x}Zn_xS$/ZnS Nanocrystals. *Chem. Mater.* **2008**, *20*, 5307−5313.
(40) Beane, G. A.; Gong, K.; Kelley, D. F. Auger and Carrier Trapping Dynamics in Core/Shell Quantum Dots Having Sharp and Alloyed Interfaces. *ACS Nano* **2016**, *10*, 3755−3765.
(41) Boldt, K.; Kirkwood, N.; Beane, G. A.; Mulvaney, P. Synthesis of Highly Luminescent and Photo-Stable, Graded Shell CdSe/$Cd_xZn_{1-x}S$ Nanoparticles by in Situ Alloying. *Chem. Mater.* **2013**, *25*, 4731−4738.
(42) Li, Z. J.; Zhang, G. F.; Li, B.; Chen, R. Y.; Qin, C. B.; Gao, Y.; Xiao, L. T.; Jia, S. T. Enhanced Biexciton Emission from Single Quantum Dots Encased in N-Type Semiconductor Nanoparticles. *Appl. Phys. Lett.* **2017**, *111*, 153106.
(43) Hu, F. R.; Lv, B. H.; Yin, C. Y.; Zhang, C. F.; Wang, X. Y.; Lounis, B.; Xiao, M. Carrier Multiplication in a Single Semiconductor Nanocrystal. *Phys. Rev. Lett.* **2016**, *116*, 106404.
(44) McGuire, J. A.; Joo, J.; Pietryga, J. M.; Schaller, R. D.; Klimov, V. I. New Aspects of Carrier Multiplication in Semiconductor Nanocrystals. *Acc. Chem. Res.* **2008**, *41*, 1810−1819.
(45) Hu, F. R.; Zhang, H. C.; Sun, C.; Yin, C. Y.; Lv, B. H.; Zhang, C. F.; Yu, W. W.; Wang, X. Y.; Zhang, Y.; Xiao, M. Superior Optical Properties of Perovskite Nanocrystals as Single Photon Emitters. *ACS Nano* **2015**, *9*, 12410−12416.
(46) Yuan, G. C.; Ritchie, C.; Ritter, M.; Murphy, S.; Gomez, D. E.; Mulvaney, P. The Degradation and Blinking of Single $CsPbI_3$ Perovskite Quantum Dots. *J. Phys. Chem. C* **2018**, *122*, 13407−13415.

(47) Kuno, M.; Fromm, D. P.; Hamann, H. F.; Gallagher, A.; Nesbitt, D. J. On"/"Off" Fluorescence Intermittency of Single Semiconductor Quantum Dots. *J. Chem. Phys.* **2001**, *115*, 1028−1040.
(48) Jin, S. Y.; Song, N. H.; Lian, T. Q. Suppressed Blinking Dynamics of Single QDs on ITO. *ACS Nano* **2010**, *4*, 1545−1552.
(49) Zhang, G. F.; Yang, C. G.; Ge, Y.; Peng, Y. G.; Chen, R. Y.; Qin, C. B.; Gao, Y.; Zhang, L.; Zhong, H. Z.; Zheng, Y. J.; Xiao, L. T.; Jia, S. T. Influence of Surface Charges on the Emission Polarization Properties of Single CdSe/CdS Dot-in-Rods. *Front. Phys.* **2019**, *14*, 63601.
(50) Li, B.; Zhang, G. F.; Yang, C. G.; Li, Z. J.; Chen, R. Y.; Qin, C. B.; Gao, Y.; Huang, H.; Xiao, L. T.; Jia, S. T. Fast Recognition of Single Quantum Dots from High Multi-Exciton Emission and Clustering Effects. *Opt. Express* **2018**, *26*, 4674−4685.
(51) Nair, G.; Zhao, J.; Bawendi, M. G. Biexciton Quantum Yield of Single Semiconductor Nanocrystals from Photon Statistics. *Nano Lett.* **2011**, *11*, 1136−1140.
(52) Hou, X. Q.; Li, Y.; Qin, H. Y.; Peng, X. G. Effects of Interface-Potential Smoothness and Wavefunction Delocalization on Auger Recombination in Colloidal CdSe-Based Core/Shell Quantum Dots. *J. Chem. Phys.* **2019**, *151*, 234703.
(53) Qin, H. Y.; Meng, R. Y.; Wang, N.; Peng, X. G. Photoluminescence Intermittency and Photo-Bleaching of Single Colloidal Quantum Dot. *Adv. Mater.* **2017**, *29*, 1606923.
(54) Ebenstein, Y.; Mokari, T.; Banin, U. Fluorescence Quantum Yield of CdSe/ZnS Nanocrystals Investigated by Correlated Atomic-Force and Single-Particle Fluorescence Microscopy. *Appl. Phys. Lett.* **2002**, *80*, 4033−4035.

https://dx.doi.org/10.1021/acs.jpclett.0c03065
J. Phys. Chem. Lett. 2021, 12, 405−412